

## Article

# Calculation of NH<sub>3</sub> Emissions, Evaluation of Backward Lagrangian Stochastic Dispersion Model and Aerodynamic Gradient Method

Jesper Nørlem Kamp <sup>1,\*</sup> , Christoph Häni <sup>2</sup> , Tavs Nyord <sup>1</sup>, Anders Feilberg <sup>1</sup>  and Lise Lotte Sørensen <sup>3</sup>

<sup>1</sup> Air Quality Engineering, Department of Biological and Chemical Engineering, Aarhus University, 8200 Aarhus N, Denmark; tavs.nyord@bce.au.dk (T.N.); af@bce.au.dk (A.F.)

<sup>2</sup> School of Agricultural, Forest and Food Sciences HAFL, Bern University of Applied Sciences, 3052 Zollikofen, Switzerland; christoph.haeni@bfh.ch

<sup>3</sup> Department of Environmental Science, Aarhus University, 4000 Roskilde, Denmark; lls@envs.au.dk

\* Correspondence: jk@bce.au.dk

**Abstract:** Two campaigns measuring ammonia (NH<sub>3</sub>) emissions with different measurement techniques were performed on a large grass field (26 ha) after the application of liquid animal manure. The aim was to compare emissions from a confined area estimated from either (i) concentration measurements, both point and line-integrated measurements, combined with backward Lagrangian stochastic (bLS) dispersion modeling or by (ii) estimation of the vertical flux by the aerodynamic gradient method (AGM) with and without footprint correction approximated by the bLS model estimates of the flux footprint. The objective of the comparison is to establish the best practice to derive NH<sub>3</sub> emissions from a large field. NH<sub>3</sub> emissions derived from bLS agreed well when comparing point and line-integrated measurements. Simple point measurements combined with bLS yield good emission estimations for the confined area. Without footprint correction, the AGM underestimates the emissions by up to 9% compared to the footprint-corrected AGM results. The sensitivity of the measurement methods makes it possible to quantify NH<sub>3</sub> emissions with diurnal patterns even five days after a field application of liquid animal manure under wet conditions. The bLS model proves to be a strong tool to determine the NH<sub>3</sub> emissions from point concentration measurements inside a large field after a slurry application.

**Keywords:** ammonia emission; backward Lagrangian stochastic model; micrometeorological techniques; differential optical absorption spectroscopy; cavity ring-down spectroscopy; grassland



**Citation:** Kamp, J.N.; Häni, C.; Nyord, T.; Feilberg, A.; Sørensen, L.L. Calculation of NH<sub>3</sub> Emissions, Evaluation of Backward Lagrangian Stochastic Dispersion Model and Aerodynamic Gradient Method. *Atmosphere* **2021**, *12*, 102. <https://doi.org/10.3390/atmos12010102>

Received: 10 December 2020

Accepted: 6 January 2021

Published: 12 January 2021

**Publisher's Note:** MDPI stays neutral with regard to jurisdictional claims in published maps and institutional affiliations.



**Copyright:** © 2021 by the authors. Licensee MDPI, Basel, Switzerland. This article is an open access article distributed under the terms and conditions of the Creative Commons Attribution (CC BY) license (<https://creativecommons.org/licenses/by/4.0/>).

## 1. Introduction

Ammonia (NH<sub>3</sub>) emission from the agricultural sector has attracted considerable attention in recent decades due to the negative effect on human health and the environment, with the eutrophication and acidification of local water, as well as negative effects on biodiversity [1–3]. Furthermore, NH<sub>3</sub> is also a precursor for aerosols, which harm human health and affect global warming [4], and NH<sub>3</sub> is also an indirect source of nitric oxide and the potent greenhouse gas nitrous oxide [5]. Increased demand for food with a growing population pushes the production with a need for nitrogen-based fertilizers in nitrogen-limited ecosystems. The agricultural sector accounts for 94% of NH<sub>3</sub> emissions in Europe with field applications of liquid animal manure (slurry) as the largest source [6]. The Gothenburg Protocol to Abate Acidification, Eutrophication and Ground-level Ozone from 1999 regulates NH<sub>3</sub> emissions, which commits member countries to calculate and report annual emissions [7]. It is crucial to have accurate and well-tested flux measurement techniques available to quantify NH<sub>3</sub> emissions and document emission reductions by the assessment of technological improvements in the agricultural sector.

Ammonia flux measurements have often been determined from measurements with passive samplers or denuders, methods that are labor-intensive and provide low temporal

resolution [8–11]. More recently,  $\text{NH}_3$  flux has been determined by the direct turbulence flux method eddy covariance (EC), which requires fast (often 10 Hz) concentration measurements by Proton Transfer Reaction-Mass Spectrometer (PTR-MS) [12] and with Tunable Infrared Laser Differential Absorption Spectrometry (TILDAS) [13]. Due to wall adsorption in the inlet lines and partitioning with adsorbed water, these systems can experience significant dampening of the high-frequency response fluctuations, which will underestimate  $\text{NH}_3$  fluxes [14]. It is a common problem for  $\text{NH}_3$  measurements that the high polarity and water solubility of  $\text{NH}_3$  cause adsorption to most surfaces [15]. Open path optical measurement is a possible solution to avoid the adsorption of  $\text{NH}_3$ , but available open path instruments for  $\text{NH}_3$  are not capable of performing measurements sufficiently fast for EC. Dampening might be overcome by using spectral analysis and data filter methods [16]. An open path system is described by Sintermann et al. [17] that uses differential optical absorption spectroscopy (miniDOAS) to measure line-integrated  $\text{NH}_3$  concentrations. A backward Lagrangian stochastic (bLS) dispersion model deduced by Flesch et al. [18] can be applied to the miniDOAS concentration to derive the emission rate from a ground source. The software WindTrax ([www.thunderbeachscientific.com](http://www.thunderbeachscientific.com)) is a direct product of this bLS model [18], which has also been developed as a bLS model package in the software R [19]. The bLS model and miniDOAS instruments have been used in a controlled release experiment, with  $\text{NH}_3$  showing a general underestimation of  $\text{NH}_3$  emissions for concentration measurements spatially separated from the source area when dry deposition is not taken into account [19]. This underestimation due to dry deposition also applies to flux footprint calculations in micrometeorological methods such as EC and the aerodynamic gradient method (AGM) that estimate fluxes from a footprint area by vertical flux measurements if the source is separated from the measurement site. A dry deposition will only have a very limited effect on measurements at the edge of or inside the source area. The AGM is a micrometeorological method based on similarity theory (K-theory) to determine fluxes from concentration measurements at a minimum of two heights. The implications of discontinuous AGM measurements with a single analyzer were examined with data from this presented study [20]. The concentration measurements and meteorological parameters are averaged to determine fluxes in the averaging interval, e.g., half-hourly  $\text{NH}_3$  fluxes [21]. The averaging allows for using low response analyzers to measure the concentration, since the measurement frequency is much less of a limitation. Consequently, lower detection limits can be reached, and a wider range of compounds can be measured when using AGM and bLS.

Micrometeorological methods can be used to determine the flux for an infinite area with horizontal homogeneity, but often, this assumption is difficult to meet. The bLS model approach, however, takes the geometry of the source into account.

The bLS dispersion model will be used in this work to correct  $\text{NH}_3$  emission measurements for the footprint exceeding the area of interest when using the AGM in order to determine  $\text{NH}_3$  emissions from a large grass field after slurry application. The bLS model is well-documented [18,22,23]—in particular, with line-integrated concentration measurements upwind and downwind. The measurement position (i.e., inside or outside the source) has been evaluated previously on a 1-ha rectangular field with long sampling intervals against the integrated horizontal flux method (IHF) [24]. Comparison of  $\text{NH}_3$  from EC and bLS flux from measurements inside the source area on 1.23 and 0.77-ha fields show good agreement between the methods [25]. To our knowledge, no studies have investigated ammonia fluxes with AGM and bLS measurements on a large field with complex geometry. Other studies measured inside smaller fields or plots, e.g.,  $30 \times 30$  m [26] and 2.7 and 2.8 ha [27]; thus, the use of bLS with point measurements inside a source area have been conducted previously. This study compares AGM and bLS with point and line-integrated concentration measurements for the feasibility to determine  $\text{NH}_3$  emissions from a large field (26 ha). Point measurement inside the source area combined with bLS might be a good alternative to the commonly used AGM or the (for  $\text{NH}_3$ ) more costly EC

method for a large field with complex geometry, and the study presented here will focus on the evaluation of the best practice for measuring emission rates from a large field.

## 2. Materials and Methods

### 2.1. Site Description

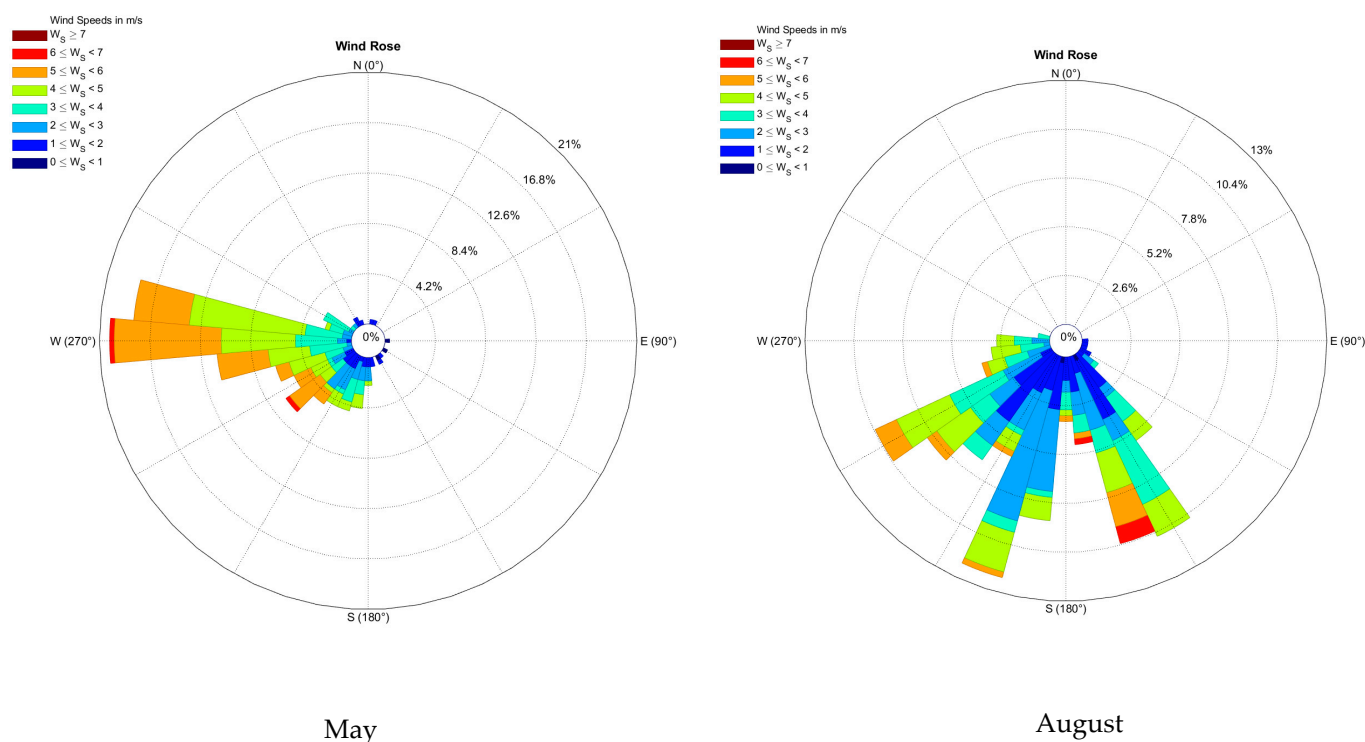
The field site ( $56^{\circ}27'12''$  N,  $9^{\circ}32'26''$  E) is a 26-ha grass field located in Central Jutland in Denmark, 63 m a.s.l. Two separate measurement campaigns were conducted at the same site, in May and August 2019, directly after slurry application. The grass was cut 3 days before both experiments and had an average height of 15 cm for both campaigns. Slurry application started in the morning, mainly going from west to east on the field, and lasted almost 10 h (see Figure 1). The slurry application rate was 30 ton/ha and 35 ton/ha in May and August, respectively (see Table 1). The applications exceeded the fertilization limit of  $170 \text{ kg N ha}^{-1}$ , but Danish and EU legislation allows  $230 \text{ kg N/ha}$  for cattle farming, with much grass in the crop rotation. The application of the slurry was done by open slot injection, with a so-called “double-disc injector”, operating in approximately 4 cm below the soil surface and row spacing of approximately 17 cm. The slots were, for the most part, able to contain the volume of applied slurry. Digested slurry from a biogas plant based on mainly cattle manure but also including swine, poultry, and mink manure was used; see the composition in Table 1. The biogas plant was operated at a temperature of  $53^{\circ}\text{C}$  and a hydraulic retention time (HRT) of 13 days [28]. The same source of slurry was used in both campaigns but from two different periods. The soil was ordinary agricultural land in rotation with the USDA soil classification sandy loam soil and an organic matter content below 5% (*w/w*). A measuring tower was positioned in the middle of the field approximately 200 m from the nearest obstacle in any direction (see Figure 1). The tower had the same position on the field for both campaigns, and the wind directions during both campaigns are seen in Figure 2.



**Figure 1.** Overview of the field and measurement location on the field. The colored area is the 26-ha field where slurry was applied. MD-W and MD-E are the differential optical absorption spectroscopy (miniDOAS) located west and east, respectively, the tower includes the micrometeorological measurements and point concentration measurement of ammonia ( $\text{NH}_3$ ) with cavity ring-down spectroscopy (CRDS).

**Table 1.** Slurry composition in May and August of the digested slurry from a biogas plant.

Measurement Period	Dry Matter (%)	Total kg N $\text{ton}^{-1}$	Kg $\text{NH}_4^+\text{-N}$ $\text{ton}^{-1}$	Phosphorus (kg $\text{ton}^{-1}$ )	Potassium (kg $\text{ton}^{-1}$ )	pH	Application Rate ( $\text{ton ha}^{-1}$ )
May	5.35	3.10	1.80	0.47	2.06	7.8	30
August	3.31	2.79	1.62	0.36	1.78	7.7	35

**Figure 2.** Wind direction and speed for the measurement campaigns in May (left) and August (right).

## 2.2. Instrumentation

Measurements were carried out from 21–27 May 2019 (136 h) and 14–21 August 2019 (160.5 h). An ultrasonic anemometer (METEK GmbH, Elmshorn, Germany, uSonic-3 Scientific) was installed at 2-m height in the tower to measure the 3-dimensional wind components and temperature at 10-Hz resolution from which wind speed, wind direction, friction velocity, and stability in terms of the Obukhov length were calculated. Two cavity ring-down spectroscopy (CRDS) analyzers from Picarro model G2103 (Picarro Inc., Santa Clara, CA, USA) were used to measure  $\text{NH}_3$  and  $\text{H}_2\text{O}$  concentrations at 1 m and 2 m. The study by Kamp et al. [29] investigated this specific CRDS instrument for use in an agricultural environment and found only negligible interference from volatile organic compounds (VOCs) over a wide concentration range and reported a standard deviation of  $0.08 \mu\text{g m}^{-3}$  giving a limit of detection of  $0.24 \mu\text{g m}^{-3}$  (three times the standard deviation). During setup, the two CRDS instruments used measured side-by-side the ambient air in the field before both of the measurement campaigns for comparison and correction of the instruments. The concentration span was 6–10  $\mu\text{g m}^{-3}$ .

A trailer was placed east of the tower, and the CRDS analyzers were placed inside the trailer. Two insulated 10-m polytetrafluoroethylene (PTFE) tubes heated to approximately  $40^\circ\text{C}$  were used for the inlets of the  $\text{NH}_3$  CRDS, and they were attached to the tower at 1 m and 2 m, respectively. The response time of a system with the same type of heated tubes (up to 50 m) was 5–25 s [29]. The trailer was placed in the least prevailing wind direction to avoid disturbances of the measurements. During both campaigns, the inlet tubes of the two  $\text{NH}_3$  CRDS analyzers were swapped several times to avoid instrumental bias.

Two miniDOAS instruments developed by Sintermann et al. [17] were used to measure  $\text{NH}_3$  concentrations in the ambient air during the campaign in August. The miniDOAS instruments are open path analyzers that measure concentrations from line-integrated averages by UV absorption between a light source and a detector [19]. In practice, the path length is doubled by a retroreflector; thus, the light source and the detector are in the same temperature-stabilized box. The miniDOAS instruments are described in detail by Sintermann et al. [17]. They recorded UV light spectra in the range of 200 to 230 nm and evaluated them against a reference spectrum (null spectrum). Thus, the DOAS technique provides concentration measurements above the average concentration that are related to the reference spectrum. Spectra were recorded every 60 to 250 ms and aggregated to one-minute averages for each instrument. The reference spectrum is preferably measured during a period in which concentrations are low and optical transmission, therefore, is relatively high. The reference spectrum for the miniDOAS evaluation was recorded on 11.08.2019 between 21:30 and 22:30 local time, when the instruments were standing side-by-side with a path length of 70 m overnight. The concentration during the reference period was set to  $2.5 \mu\text{g m}^{-3}$  for  $\text{NH}_3$ . The random uncertainty in the miniDOAS concentration measurements is 1.4% of the concentration and not better than  $0.2 \mu\text{g m}^{-3}$  [17].

The instruments were installed at the field edges on the west and east sides of the field, respectively (Figure 1). The measurement height was 1.60 m for both instruments, and the total measurement path lengths were 73 m (west) and 75 m (east).

The background concentration was measured by the miniDOAS in the west or east side of the field, depending on the wind direction. The mean background concentration from the miniDOAS instruments was  $2.1 \pm 0.3 \mu\text{g m}^{-3}$ . If the number of touchdowns inside the source area in the bLS model is higher than an arbitrarily chosen threshold (here, 2000 touchdowns inside), the miniDOAS background concentration is assumed to be affected too strongly by the emission of the field, and a fixed background concentration of  $2.0 \mu\text{g m}^{-3}$  is used. The fixed background concentration is based on the measurements of the background concentration both with the miniDOAS but, also, from the CRDS concentrations measured at the end of the measurements campaigns.

Concentration measurements at which the light paths of the devices were not aligned well and the received light by the detectors was low (less than 15% of the initial intensity) were removed.

### 2.3. Estimation of $\text{NH}_3$ Emission Rates

The emission rate of  $\text{NH}_3$  is determined in half-hour intervals using vertical flux measurements, as well as concentration measurements in combination with dispersion modeling. There are mainly two options for estimating the emission rate of a scalar from a source when taking the dispersion of the scalar into account. The first option is to measure the vertical flux at a given location in the emission plume and relate the measured flux to the emission rate by using a dispersion model (here, flux footprint) that calculates the ratio between the source strength (emission rate) and the measured flux. This flux-to-emission rate ratio corresponds to the integration of the flux footprint over the emitting source area. This ratio will converge towards one with an increasing extent of the upwind source area, which often can be assumed negligibly close to one in practice; thus, the dispersion modeling is redundant in such a case. For the flux footprint, it is a commonly used rule of thumb that the upwind terrain must have a uniform fetch equal to 100 times the measurement height, as the footprint area increases with the measurement height [30]. The second option is equivalent, but the measured quantity is the average concentration instead of the vertical flux. The measured concentration is related to the emission rate by a dispersion (here, concentration footprint) model that calculates the ratio between the emission rate and the measured concentration. The concentration-to-emission rate ratio corresponds to the integration of the concentration footprint over the emitting source area. Note that the concentration footprint does not integrate to one, as the flux footprint, in the case of an infinite source area and its value (unit  $\text{s m}^{-1}$ ) is dependent on the turbulent state

of the atmosphere. The footprint area is specific for atmospheric conditions and surface characteristics [31].

Two different approaches to estimate the NH<sub>3</sub> fluxes from the source area (i.e., emission rates) were used:

- (1) measurement of the vertical NH<sub>3</sub> flux by the AGM in combination with a flux footprint model and
- (2) measurement of the NH<sub>3</sub> concentration in combination with a concentration footprint model.

#### 2.4. Aerodynamic Gradient Method

The AGM-estimated fluxes are based on Fick's law [30]:

$$F = -K_c \frac{\partial c}{\partial z} \quad (1)$$

where  $F$  is the NH<sub>3</sub> flux ( $\mu\text{g m}^{-2} \text{s}^{-1}$ ),  $K_c$  is the eddy diffusivity ( $\text{m}^2 \text{s}^{-1}$ ), and  $\partial c / \partial z$  is the vertical concentration gradient of NH<sub>3</sub> ( $\mu\text{g m}^{-3} \text{m}^{-1}$ ). By convention, a positive flux denotes emission, and a negative flux denotes deposition. This relationship between the vertical gradient of the concentration and the vertical flux can be parameterized based on the Monin-Obukhov similarity theory (MOST) to [32]:

$$F = -K_c \frac{\partial c}{\partial z} = \frac{u_* k (c_2 - c_1)}{\ln\left(\frac{z_2}{z_1}\right) - \psi_{c,2} + \psi_{c,1}} \quad (2)$$

where  $u_*$  is the friction velocity ( $\text{m s}^{-1}$ ),  $k$  is the unitless von Karman constant (0.4),  $z_2$  and  $z_1$  are upper and lower inlet heights, respectively, (m),  $c_2$  and  $c_1$  are the NH<sub>3</sub> concentrations measured at heights  $z_2$  and  $z_1$  ( $\mu\text{g m}^{-3}$ ), and  $\psi_{c,2}$  and  $\psi_{c,1}$  are the stability correction functions for scalars at heights  $z_2$  and  $z_1$ . Stability correction functions from Dyer and Hicks [33] were used. The friction velocity and the Obukhov length, which are employed in the stability correction functions, were calculated with data from the ultrasonic anemometer. The concentration measurements from the two CRDS instruments were used to calculate the concentration difference between 1 m and 2 m. This study used the flux footprint of the bLS model at the geometric mean height to correct the AGM emission.

#### 2.5. Dispersion Modeling

The employed bLS model [18] is embedded in the software R [19]. It is used to model the concentration-to-emission rate ratio ( $\text{CE}_{\text{bLS}}$ ) and the vertical flux-to-emission rate ratio ( $\text{wCE}_{\text{bLS}}$ ) [34] for the duration of a measurement interval at a specific location (sensor) relative to a confined source area. The model calculates upwind (backward in time) trajectories released at the position of the sensor based on the provided turbulence field. A set of touchdown locations, where the backward trajectories touch the surface and vertical (touchdown) velocities at impact are used to calculate the model output. Only the touchdowns within the source are used. The number of trajectories can be increased to raise the number of touchdowns inside the source area and thereby improve the model estimate. The source area is assumed to have a spatially homogeneous emission that is constant in time, at least during each averaging interval. For each averaging interval—here, 30 min—the following inputs are required: the friction velocity  $u^*$  ( $\text{m s}^{-1}$ ); the roughness length  $z_0$  (m); the Obukhov length  $L$  (m); the standard deviation of the wind components normalized by the friction velocity  $\sigma_u$ ,  $\sigma_v$ , and  $\sigma_w$  ( $\text{m s}^{-1}$ ); and the wind direction. The bLS model takes the geometry of the emitting source into account; thus, the geometry of the source area and the location of the concentration sensors are required inputs as well, e.g., with GPS coordinates outlining the source and positions for the sensors. The  $\text{CE}_{\text{bLS}}$  and  $\text{wCE}_{\text{bLS}}$  values are calculated for each sensor and source for each averaging interval. In the most frequently used case of bLS modeling and concentration measurements, the average

emission rate  $E$  in an interval is calculated by combining the concentration measurements with the expected ratios from the bLS model:

$$E = (C_{downwind} - C_{upwind}) / CE_{bLS} \quad (3)$$

where  $C_{downwind}$  is the concentration measured downwind from (i.e., in the plume of) the source, and  $C_{upwind}$  is the inflow (background) concentration measurement that is unaffected by the source emission itself.

The relation between the vertical flux ( $F_{AGM}$ ; here, measured by using the AGM) and the emission rate  $E$  is given by:

$$E = F_{AGM} / wCE_{bLS} \quad (4)$$

Thus, the emissions from the AGM flux measurements are corrected for footprint contribution to the flux and will be called footprint-corrected AGM flux.

The friction velocity,  $u_*$ , is used as a quality control factor for the bLS estimate, since, according to Flesch et al. [18],  $u_*$  is the single best factor for the bLS model by eliminating cases with  $u_* \leq 0.15 \text{ m s}^{-1}$ . This will remove data with low winds, where the assumptions of horizontal homogeneity and stationarity might be violated [18]. Furthermore, intervals with extreme stability can violate the assumptions of MOST; thus, data with  $|L| \leq 10$  was rejected [35]. The intervals where the roughness length,  $z_0$ , was either  $\leq 1/100$  of the canopy height or  $\geq 1/3$  of the canopy height were rejected. For the two campaigns, 23 of 257 and 75 of 320 half-hour periods were removed for May and August, respectively, with the three filtering criteria mentioned above. For the two CRDS point measurements, 1 million trajectories were calculated for each averaging interval in the bLS model. The modeling of the line-integrated miniDOAS measurements was approximated by 30 point sensors equally distributed over the measurement path of the instruments. The trajectories (50,000) were calculated for each release point.

In May and August, the slurry application lasted almost 10 h; thus, there were spatial variations of the emissions over the field. The campaigns started when the slurry application was completed. The emissions started directly after slurry application; thus, the field was not one homogenous emitting source. To overcome this issue, the field was separated into four sources in the bLS model. The contribution of each sub-source to the total emissions from the entire field was calculated based on the temporal emission development estimated by the Ammonia Loss from Field-Applied Manure (ALFAM2) model considering the time since slurry application, slurry parameters, and weather data for each half-hour interval [36].

### 3. Results

At two measurement campaigns in May and August (2020), the  $\text{NH}_3$  emissions were measured directly after slurry application. The emission was highest directly after slurry application and decreased over time with diurnal variations, as seen in Figures 3 and 4. The lowest fluxes were observed at the very end of the measurements in May and four days after application during rainfall in August. Depending on the method, the highest emissions were 7.7 to 9.4  $\mu\text{g m}^{-2} \text{ s}^{-1}$  in May and 17.5 to 39.1  $\mu\text{g m}^{-2} \text{ s}^{-1}$  in August, whereas the minimum emissions were  $-0.06 \mu\text{g m}^{-2} \text{ s}^{-1}$  in May and  $-0.08 \mu\text{g m}^{-2} \text{ s}^{-1}$  in August. In general, the emissions were highest between 9.00 and 12.00 and lowest between 21.00 and 00.00. The mean emission (see Table 2) was highest in August, and in general, the emission estimations from bLS were higher than from the AGM. The bLS model is used as a footprint model to estimate how much of the area outside the field contributes to the flux measured by the AGM, thereby allowing for correction of the AGM flux. If the footprint area for the AGM measurements is larger than the field of interest, part of the flux will come from areas with emission rates that differ from the field emission rate. This introduces an unknown bias into the estimated field emission rate. For a field of infinite size, there would be no correction to the AGM. The mean AGM emission corrected by the

bLS model is higher than the uncorrected emission, as is seen in Table 2, but lower than the corresponding emissions estimated from concentration measurements in combination with the bLS model.

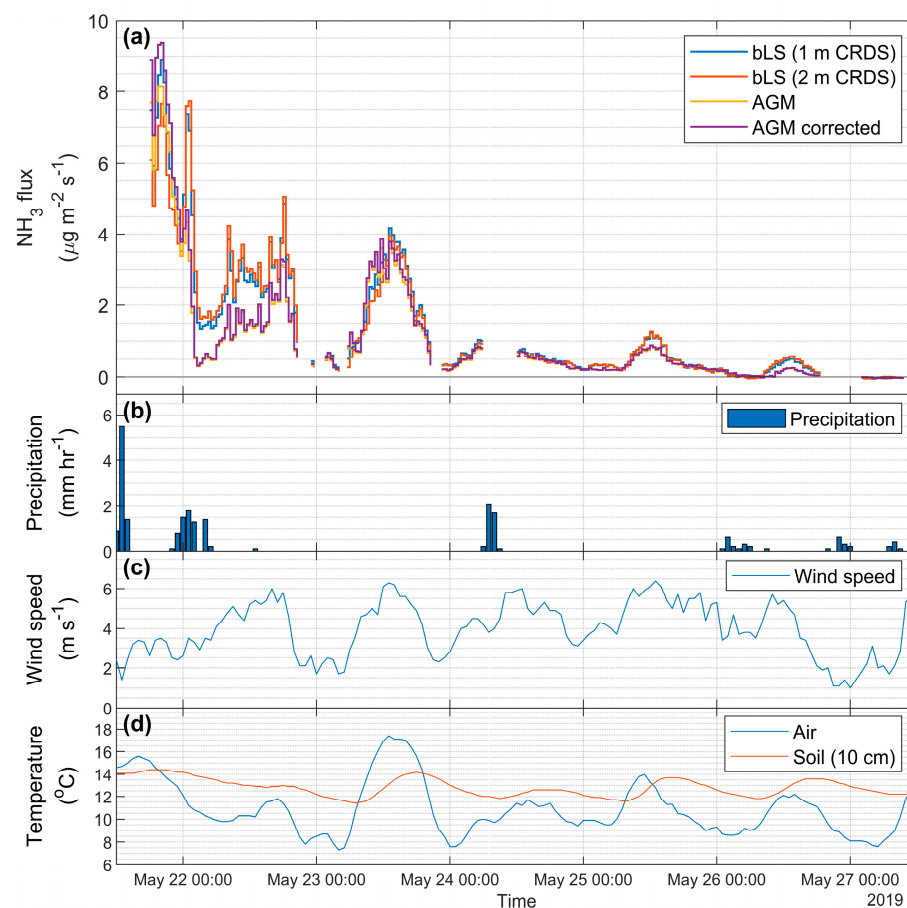


**Figure 3.** (a) Source emission of  $\text{NH}_3$  from the measurement campaign in May presented for backward Lagrangian stochastic (bLS) (1-m CRDS), bLS (2-m CRDS), the aerodynamic gradient method (AGM), and the AGM with footprint correction. (b) Precipitation per hour, (c) wind speed at 10 m, and (d) air temperature and soil temperature at 10 cm. Data in (b–d) are recorded 5 km NE of the field.

**Table 2.** Mean emissions of the measurement campaigns in May and August in  $\mu\text{g m}^{-2} \text{s}^{-1}$  for filtered data over the measurement period. AGM: aerodynamic gradient method, bLS: backward Lagrangian stochastic, CRDS: cavity ring-down spectroscopy, and miniDOAS: differential optical absorption spectroscopy.

Method	Mean Emission ( $\mu\text{g m}^{-2} \text{s}^{-1}$ )	
	May	August
AGM	1.05	1.40
AGM (footprint-corrected)	1.13	1.53
bLS (1-m CRDS)	1.38	2.05
bLS (2-m CRDS)	1.33	2.00
bLS (miniDOAS)	-	2.58

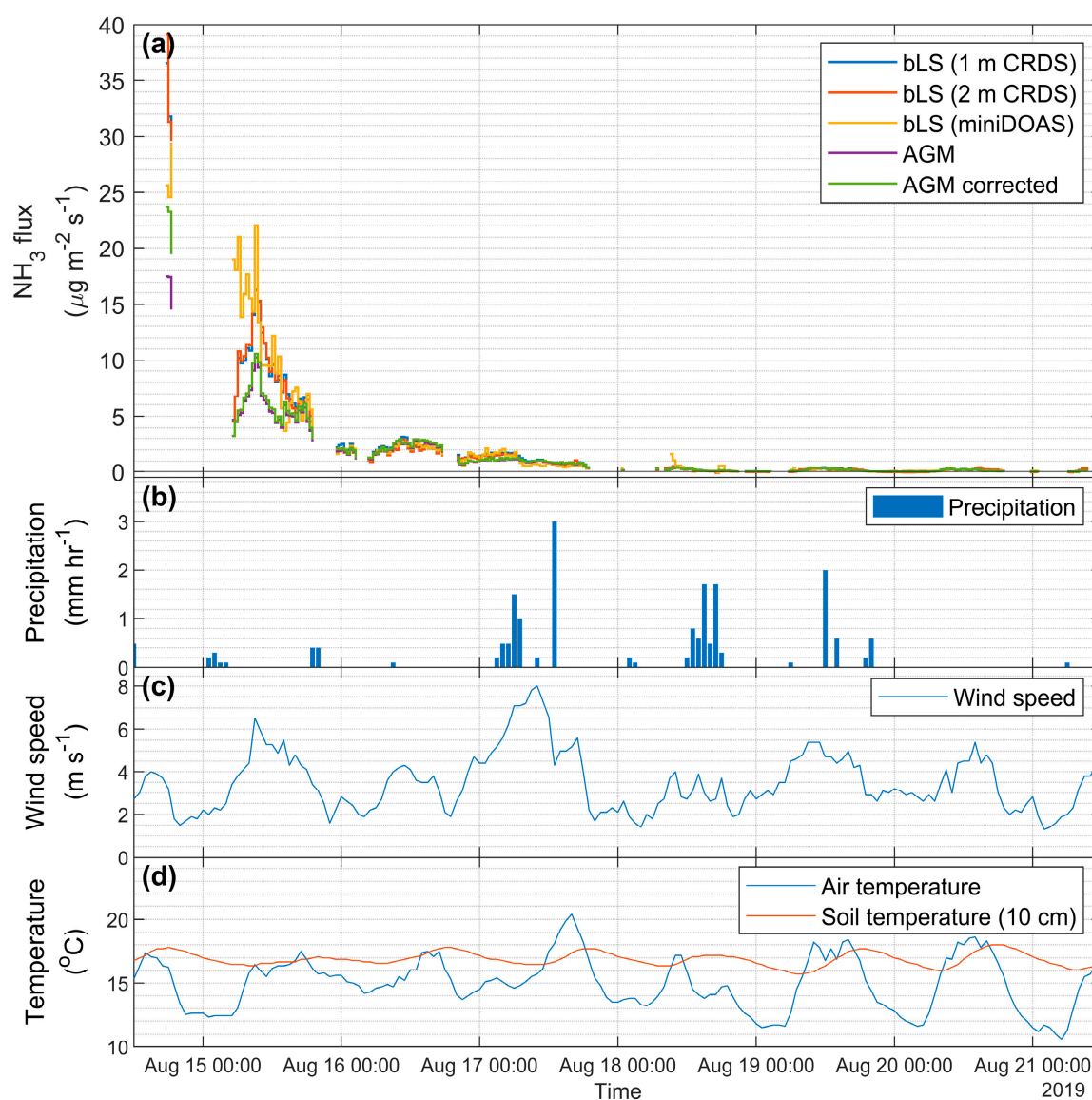


**Figure 4.** (a) Source emission of  $\text{NH}_3$  from the measurement campaign in August presented for bLS (1-m CRDS), bLS (2-m CRDS), bLS (miniDOAS), the AGM, and the AGM with footprint correction. (b) Precipitation per hour, (c) wind speed at 10 m, and (d) air temperature and soil temperature at 10 cm. Data in (b–d) are recorded 5 km NE of the field.

During the campaigns, the mean wind speed and direction were  $249^\circ$  and  $3.9 \text{ m s}^{-1}$  in May and  $197^\circ$  and  $3.0 \text{ m s}^{-1}$  in August; this is shown in Figure 2. The mean temperatures were  $11.3 \text{ }^\circ\text{C}$  and  $14.5 \text{ }^\circ\text{C}$  in May and August, respectively. The mean of the stability parameter  $z/L$  was  $-0.005$  in May and  $0.003$  in August. Division into stability classes for the averaging intervals showed most cases with neutral conditions (48%) in May, followed by unstable (39%) and stable (13%) conditions, whereas most cases were with unstable conditions (41%) in August, followed by stable (34%) and neutral (25%).

The footprint correction of the AGM increases the measured mean emissions (Table 2) by 8 to 9% for the two measurement campaigns, but even for the corrected AGM flux, the mean emissions are 15% and 41% lower than the CRDS-bLS and miniDOAS-bLS measurements, respectively. The total ammoniacal nitrogen (TAN) loss is 21–32% lower for the AGM compared to CRDS-bLS, and the footprint-corrected AGM is 15–25% lower than CRDS-bLS.

The relative loss of total ammoniacal nitrogen (% of TAN) from the field estimated from the total amount of TAN in the applied slurry is presented in Table 3. The miniDOAS dataset has some large gaps without data, and no gap filling is done; thus, the total loss of

TAN estimated from the miniDOAS is not reported. The total loss of TAN estimated from the bLS model emissions and AGM emissions in Table 2 is lower than the true loss, because the measurements did not start until the slurry was applied to the whole field. Thus, the very first emissions from the first part of the field are not registered by the measurements. The loss of TAN from the AGM is lower compared to estimates from the bLS model, and the TAN loss is highest in August.

**Table 3.** Loss of total ammoniacal nitrogen (TAN) in percentage in May and August for the filtered data measurements starting after slurry was applied to the whole field over the measurement period.

Method	Loss of TAN in %	
	May	August
AGM	8.2	10.3
AGM (footprint-Corrected)	8.9	11.3
bLS (CRDS 1 m)	10.7	15.1
bLS (CRDS 2 m)	10.4	14.6

From the flux footprint (Figure 5a) and concentration footprints for 1 m (Figure 5b) and 2 m (Figure 5c), it is clear that the concentration footprints are much larger than the flux footprint, and the highest measurement level gives the largest footprint area, as expected.

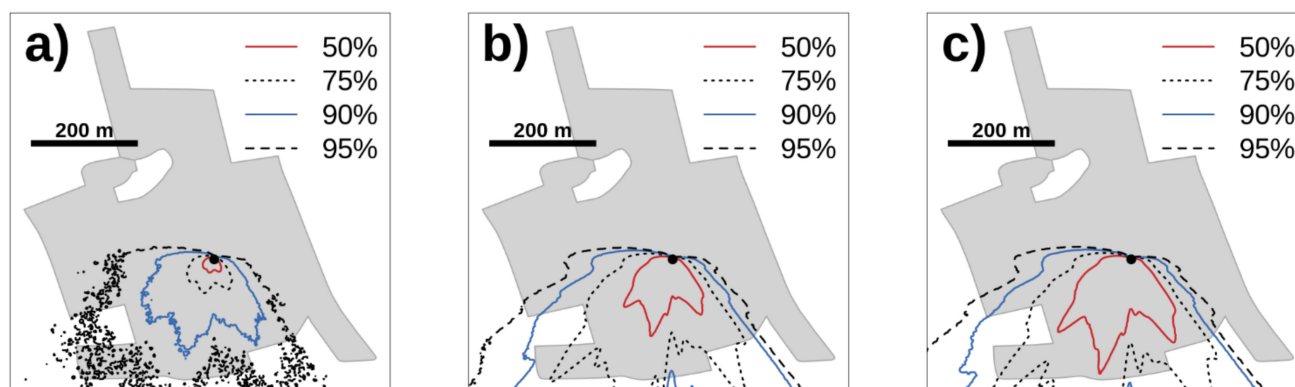
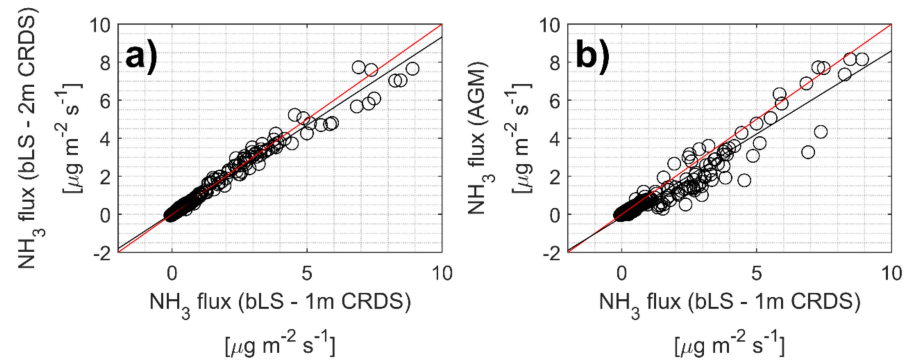


**Figure 5.** The lines represent the areas contributing to 50%, 75%, 90%, and 95% for (a) the flux footprint area, contributing to the flux measurement. The concentration footprint areas for (b) 1 m and (c) 2 m, contributing to the concentration measurements. Areas for the concentration footprints are approximated by assuming 100% of the contribution is within 750 m. The footprints are averaged over all measurement intervals in August.

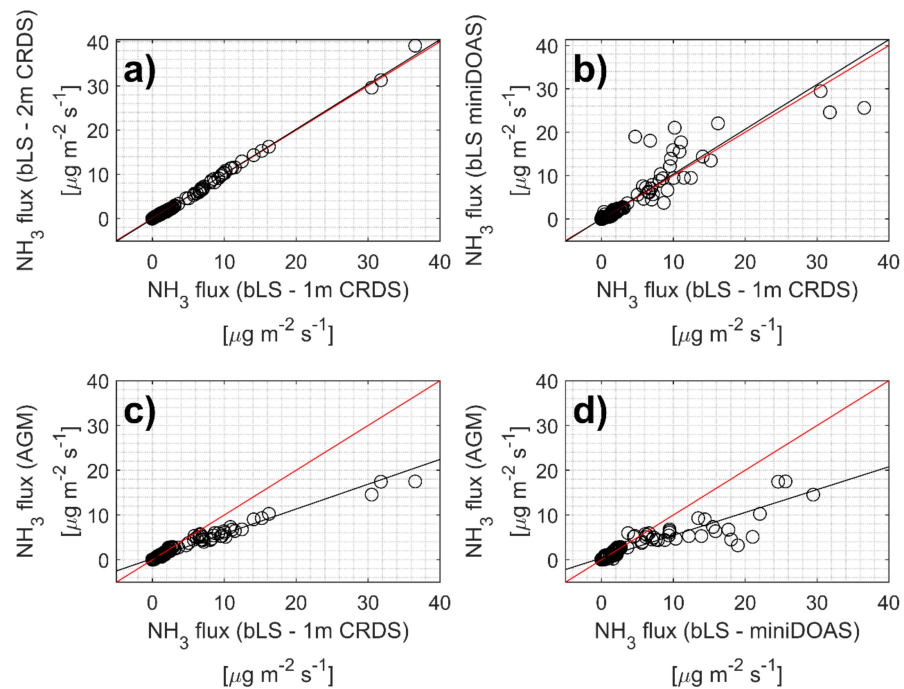
The background concentration measurements are very important for bLS when the emissions are low but do not affect the TAN loss much. The background concentration was set to  $2.0 \mu\text{g m}^{-3}$  for  $\text{NH}_3$  when no measurements were available from the miniDOAS, as described in Section 2. Changing this background concentration to  $1.0 \mu\text{g m}^{-3}$  or  $3.0 \mu\text{g m}^{-3}$  resulted in deviations relative to the mean flux and loss of the TAN of less than 5%. Furthermore, the miniDOAS reference spectrum was recorded with the concentration set to  $2.5 \mu\text{g m}^{-3}$ , and if the concentration during the reference period was  $1.5 \mu\text{g m}^{-3}$  or  $3.5 \mu\text{g m}^{-3}$ , the relative deviation would still be less than 5%.

Individual emissions for the different emission estimating methods are compared with Deming regression (see Figures 6 and 7), and the regression coefficients are in Table 4. Deming regression is used, because it treats both variables in the same way by minimizing the perpendicular distances from the data to the fitted line. Hence, Deming regression takes into account that both methods may be prone to random error. Overall, there is a good agreement between emissions estimated from concentration measurements in combination with the bLS model, as expected with slopes of  $0.93 \pm 0.02$  (CRDS-bLS 1 m and 2 m in

May),  $1.01 \pm 0.02$  (CRDS-bLS 1 m and 2 m in August), and  $1.03 \pm 0.13$  (CRDS-bLS 1 m and miniDOAS-bLS in August); see Table 4. The comparison with CRDS-bLS (1 m) has a slope of  $0.88 \pm 0.04$  and, after correction,  $0.99 \pm 0.05$  in May and a slope of  $0.55 \pm 0.03$  and, after correction,  $0.70 \pm 0.02$  in August. For the AGM comparison with miniDOAS-bLS, the slope is  $0.51 \pm 0.05$  and  $0.62 \pm 0.08$  after correction.



**Figure 6.** Correlation between the  $\text{NH}_3$  fluxes estimated by (a) CRDS-bLS 1 m and CRDS-bLS 2 m and (b) CRDS-bLS 1 m and AGM in the May campaign. The black lines are Deming regression lines, and the red lines are 1:1 lines. The regression coefficients are shown in Table 4.

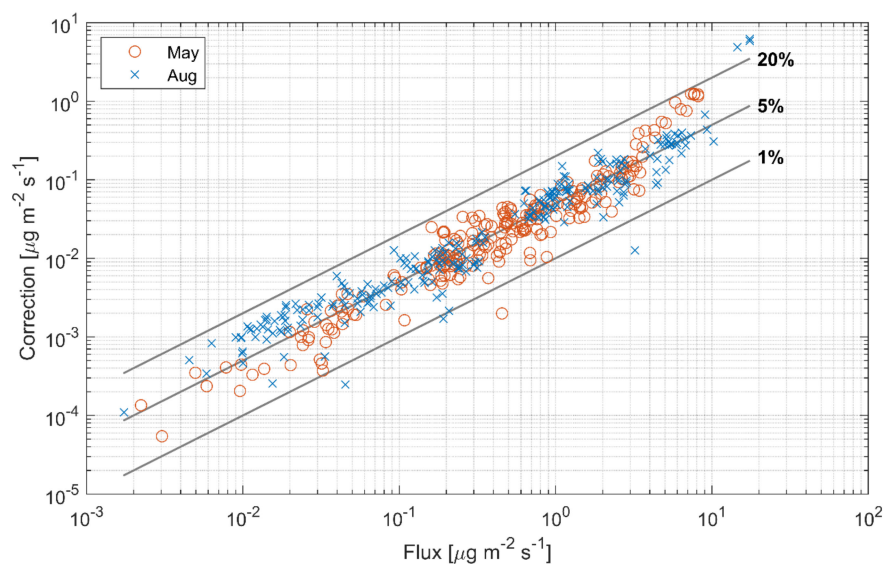


**Figure 7.** Correlation between the  $\text{NH}_3$  fluxes estimated by (a) CRDS-bLS 1 m and CRDS-bLS 2 m, (b) CRDS-bLS 1 m and miniDOAS-bLS, (c) CRDS-bLS 1 m and AGM, and (d) miniDOAS-bLS and AGM in the August campaign. The black lines are Deming regression lines, and the red lines are 1:1 lines. The regression coefficients are shown in Table 4.

The magnitude of the AGM correction based on bLS is proportional to the magnitude of the flux. The absolute magnitude of the flux exhibits a linear behavior in a log–log plot. The correction is very small when the emission is low, and three intervals in August underwent a large correction, as seen in Figure 8.

**Table 4.** Regression coefficients for Deming regression between the compared methods.

Compared Methods for Regression		Slope	Intercept	Pearson Correlation
May	bLS (1-m CRDS)      bLS (2-m CRDS)	$0.93 \pm 0.02$	$0.05 \pm 0.02$	0.988
	bLS (1-m CRDS)      AGM	$0.88 \pm 0.04$	$-0.15 \pm 0.03$	0.952
	bLS (1-m CRDS)      AGM (fp-corrected)	$0.99 \pm 0.05$	$-0.22 \pm 0.05$	0.946
August	bLS (1-m CRDS)      bLS (2-m CRDS)	$1.01 \pm 0.02$	$-0.10 \pm 0.03$	0.999
	bLS (1-m CRDS)      bLS (miniDOAS)	$1.03 \pm 0.13$	$0.01 \pm 0.20$	0.911
	bLS (1-m CRDS)      AGM	$0.55 \pm 0.03$	$0.27 \pm 0.05$	0.980
	bLS (miniDOAS)      AGM	$0.51 \pm 0.05$	$0.38 \pm 0.07$	0.910
	bLS (1-m CRDS)      AGM (fp-corrected)	$0.70 \pm 0.02$	$0.16 \pm 0.03$	0.991
	bLS (miniDOAS)      AGM (fp-corrected)	$0.62 \pm 0.08$	$0.25 \pm 0.13$	0.894

**Figure 8.** Correction of the AGM emissions depending on the emission magnitude. The black lines indicate correction levels of 1%, 5%, and 20%.

#### 4. Discussion

The data from both campaigns proves the applicability of simple point concentration measurements with a limited time resolution ( $>1$  Hz) combined with bLS modeling to be capable of determining emissions for a well-defined area, as seen from the good overall agreement between CRDS-bLS and miniDOAS-bLS in Figure 7b. The computational demand for bLS is higher than for analytical footprint models, which is a downside for the method, but it demonstrates a strong method for emission determination, with a much better estimation of the footprint function close to the source [37]. The miniDOAS is considered a valid reference method that has been documented in several publications [17,19,38]. The issue of deposition during downwind transport [19] is minimized in the current setup by locating the miniDOAS at the boundary of a larger source area. The fact that miniDOAS-bLS does not provide lower emissions than CRDS-bLS further supports the hypothesis of the minimal influence of deposition, since the CRDS-bLS measures immediately above the source. However, it is also clear from Table 2, Figure 3, and Figure 7b that discrepancies between miniDOAS-bLS and CRDS-bLS occasionally occur. Relatively speaking, the discrepancies are largest for the smallest emissions, i.e., when the uncertainty of the emissions is highest.

The comparison between the miniDOAS and CRDS emission estimates from bLS also compare open and closed path systems, and, besides from some scatter appointed to the spatial position of the instruments, there is good agreement between the open and

closed path systems. The bLS model offers the possibility to use simple concentration measurements inside a source that can yield results independent of the wind direction, which is often a concern with the placement of measurement equipment upwind of the source area.

The noninvasive online measurements applied in the current study clearly demonstrate the diurnal pattern of  $\text{NH}_3$  emissions, which is lowest but still detectable during nighttime, as seen in Figures 2 and 3. Few depositional fluxes were observed, which does not agree with the bidirectional nature of the  $\text{NH}_3$  fluxes over a grassland [39], but the pattern is the same for both periods and proves an increased emission level due to slurry application even five days after slurry application. The relatively high sensitivity of the methods allows for the quantification of emissions several days after manure application, which is important, since ammonia emissions are often measured over a limited number of days. The methods used here also allow for obtaining emission estimates during periods characterized by low emissions, e.g., after rainfall, for which only limited data exist.

The comparisons of the individual half-hourly average emissions and mean emissions for the whole measurement period yielded different results with respect to the underestimation by the AGM. The mean emissions for the corrected AGM were underestimated by 15–41%, and the TAN loss was underestimated by 15–25%.

The regression slopes (Table 4) reflected the difference between the two methods and the underlying assumptions. The comparison of footprint-corrected AGM and CRDS-bLS for individual emissions in May (Figure 6b) yielded a slope close to one ( $0.99 \pm 0.05$ ). However, the results from August (Figure 7c,d) yielded slopes of  $0.70 \pm 0.02$  and  $0.62 \pm 0.08$  for footprint-corrected AGM in comparison with CRDS-bLS and miniDOAS-bLS, respectively. Even though the regressions agreed well in May for corrected AGM and CRDS-bLS, the mean emissions and loss of TAN were up to 25% and 16% lower than in August, respectively.

The AGM and bLS approaches may have different (implied) Schmidt numbers ( $Sc$ ), which will ultimately lead to different flux calculations, which can partly explain the differences between the models. Precaution regarding the  $Sc$  must be taken when using the AGM method to determine emission rates from a confined area [40].

The comparison between the emissions determined from bLS with miniDOAS and CRDS showed a slope of  $1.03 \pm 0.13$ , where the scatter was presumably due to local differences, e.g., soil dynamics, local topology, or uneven slurry distribution. The distance between the measurement equipment was approximately 200 m; thus, the emitting areas were not exactly the same.

The lower mean emission in May is ascribed to the following: (1) the mean temperature was  $3.2^\circ\text{C}$  lower in May, and (2) during slurry application in May, heavy rainfall occurred, which left the soil very wet, even with pools of water several places on the field. It has been reported that rainfall suppresses  $\text{NH}_3$  emissions [41], but even with the rainfall, the emissions were observed up to five days after application during the daytime. The suppression of  $\text{NH}_3$  emissions from rainfall could also be seen on May 22 after midnight, where a rapid decrease in the emission rates coincided with a rainfall and the lowest emissions rates observed in August after rainfall. The loss of TAN of approximately 10% applied TAN in the May experiment was surprisingly high when the timing and the amount of precipitation in the emission period were taken into account. Increasing temperatures led to increased emissions of  $\text{NH}_3$  [36,41], and higher temperatures in August and the rainfall after application in May were explanations for the difference in total loss of TAN in May and August. A higher wind speed increased the turbulent transport and, thereby, the surface exchange, which led to higher fluxes. The average wind speed was  $3.9\text{ m s}^{-1}$  in May and  $3.0\text{ m s}^{-1}$  in August; hence, the wind speed-enhanced  $\text{NH}_3$  emissions should be highest in May. A greater number of factors influenced the flux, with atmospheric parameters such as temperature, wind speed, stability, rain, humidity, and pressure and slurry composition with pH, dry matter, and temperature [36].

The emissions after cattle slurry application with splash plates have been reported to be 25% of the applied TAN on average, which is reduced by 75% with shallow injection compared to the splash plate [26]. In the August experiment, this was most probably not the case, as the loss of ammonia was approximately 20% of the applied TAN, even after open slot injection of the slurry. An explanation could be the relatively high pH of the slurry, as it was co-digested slurry. A higher pH causes higher ammonia emissions immediately after application, and this can reduce the effects of open slot injection [42]. The Danish emissions factors for TAN loss after slurry injection in a grass field is reported to be approximately 16% for pig slurry and 31% for cattle slurry during the spring and summer [43]. The TAN loss in Table 3 showed reasonable estimates, but a direct comparison with the literature is not justifiable with the differences in slurry type and composition. There were also small differences in the composition of the slurry between the two campaigns, as seen in Table 1. However, the estimates in Table 3 were lower than the true values, since the measurements started after slurry was applied to the entire field, which gave lower overall TAN losses. Nelson et al. [44] reported maximum  $\text{NH}_3$  emissions with a flux gradient system of  $2.3 \mu\text{g m}^{-2} \text{s}^{-1}$  on a cornfield treated with urea–ammonium nitrate fertilizer in water, which is of the same order of magnitude as the emissions found in this study.

The background concentration was set to  $2.0 \mu\text{g m}^{-3}$  for  $\text{NH}_3$  when it was not possible to determine a background concentration from the miniDOAS measurements. The sensitivity of the emission data on this set point was low, since the deviation relative to the mean emission and the loss of TAN were less than 5% if the background concentration was set to  $1.0 \mu\text{g m}^{-3}$  or  $3.0 \mu\text{g m}^{-3}$  instead. For the individual emissions, the background concentration had the most influence on the smallest emissions where the concentration measurement was close to the background concentration, whereas the background concentration only had limited influence on the largest individual emissions and on the averages over the whole measurement periods. The background concentration played a role in the scaling of the emissions, and the relative relationship between the emissions was still the same, even if the general background concentration level was changed, but it could potentially change the direction of the smallest fluxes. Similar low sensitivity was seen in the case of the miniDOAS reference spectrum that compared the field measurements to the reference spectrum. The deviation relative to the mean flux and the loss of TAN was less than 5% if the reference spectrum concentration was set to  $1.5 \mu\text{g m}^{-3}$  or  $3.5 \mu\text{g m}^{-3}$  instead. Even though the background set point had a small influence on the lowest emissions, it should be noted that the mini-DOAS and CRDS bLS data agreed very well at lower concentrations, as seen in Figure 4.

The fetch requirement from the rule of thumb for a measurement height of 2 m is 200 m, and the distance between the tower and the nearest obstacle was more than 200 m. However, a contribution to the AGM measurements from the area outside was very plausible, which was also confirmed by the bLS model. The CRDS concentration measurements were used to estimate emissions based on the AGM with the concentration difference between the two heights and based on the bLS model for each of the two heights; thus, there was a difference in the underlying footprint areas. The AGM used two measurement points, but the two heights had different footprint areas, and different areas contributed to the actual concentration measurements. However, this is only an issue if areas outside of the field contribute to the emission measurements, because the field is assumed a homogeneously emitting source. The footprints in Figure 5 revealed that the extension of the footprint area differed much between the methods, and it is thus important to have a homogeneously emitting source, because different areas contribute to the measurements depending on height and flux measurements methods. Inhomogeneity by spreading delay and other factors can introduce a difference in the calculated emissions that is not directly related to differences in the measurement techniques. The concentration footprint extends further than the flux footprint, as explained by Vesala et al. [45]. Approximately 90% of the flux footprint covers the same area as 50% of the concentration footprint at the same location and measurement height (2 m). Even the 75% contribution exceeds the limits of the field

for the concentration footprints, whereas 90% of the flux footprint contribution is within the source area.

The size of the correction of the AGM flux exhibited a linear relationship in a log–log plot, as seen in Figure 8. The flux magnitude generally increased with the increasing wind speed, which, on the other hand, increased the footprint area. The atmospheric stability also influenced the footprint area, and a larger footprint area corresponding to a smaller fraction of the source inside the total footprint area caused a larger correction.

## 5. Conclusions

From two measurement campaigns in May and August, it can be concluded that it is feasible to measure NH<sub>3</sub> emissions at least five days after manure applications by injection on a grass field with CRDS point measurements for the AGM and bLS, even during wet conditions. Diurnal patterns were visible for the NH<sub>3</sub> emission with maximum peaks during the daytime, and very few periods with deposition proved increased emissions five days after slurry application, even after rainfall that was characterized by low emissions.

There is a good agreement between NH<sub>3</sub> emissions estimated with bLS from point measurements with CRDS and the line measurements with miniDOAS, where the instruments are located at different heights and positions.

The AGM flux in our study was lower than the estimates from bLS. A footprint correction of AGM emissions was applied based on bLS, which increased the mean AGM emission by 8 to 9%. Point concentration measurements inside a well-defined large source area combined with bLS modeling proved to be more suitable than the AGM for NH<sub>3</sub> emission estimations.

**Author Contributions:** Conceptualization, J.N.K., C.H., and L.L.S.; methodology, J.N.K., C.H., and L.L.S.; validation, J.N.K. and C.H.; formal analysis, J.N.K. and C.H.; investigation, J.N.K.; resources, A.F., T.N., and L.L.S.; data curation, J.N.K.; writing—original draft preparation, J.N.K.; writing—review and editing, J.N.K., C.H., T.N., A.F., and L.L.S.; visualization, J.N.K. and C.H.; supervision, A.F., T.N., and L.L.S.; project administration, J.N.K. and A.F.; and funding acquisition, A.F. and T.N. All authors have read and agreed to the published version of the manuscript.

**Funding:** This research was funded by Innovation Fund Denmark, grant number 6150-00030A, and by GUPD, grant number 34009-16-1112.

**Data Availability Statement:** The data in the study are available upon request to the corresponding author (jk@bce.au.dk).

**Acknowledgments:** Thanks to technicians Bjarne Jensen, Heidi Grønbaek, and Peter Storegård Nielsen for helping with the preparation and the setup of the equipment. Thanks to the local house owners Morten and Esben for supplying us with electricity at the field. Thanks to senior advisor Michael Nørremark for measuring GPS positions on the field.

**Conflicts of Interest:** The authors declare no conflict of interest.

## References

1. Glibert, P.M. Eutrophication, harmful algae and biodiversity—Challenging paradigms in a world of complex nutrient changes. *Mar. Pollut. Bull.* **2017**, *124*, 591–606. [[CrossRef](#)] [[PubMed](#)]
2. Binzer, A.; Guill, C.; Rall, B.C.; Brose, U. Interactive effects of warming, eutrophication and size structure: Impacts on biodiversity and food-web structure. *Glob. Chang. Biol.* **2016**, *22*, 220–227. [[CrossRef](#)] [[PubMed](#)]
3. Sheppard, L.J.; Leith, I.D.; Mizunuma, T.; Cape, J.N.; Crossley, A.; Leeson, S.; Sutton, M.A.; van Dijk, N.; Fowler, D. Dry deposition of ammonia gas drives species change faster than wet deposition of ammonium ions: Evidence from a long-term field manipulation. *Glob. Chang. Biol.* **2011**, *17*, 3589–3607. [[CrossRef](#)]
4. Aneja, V.P.; Roelle, P.A.; Murray, G.C.; Southerland, J.; Erisman, J.W.; Fowler, D.; Asman, W.A.H.; Patni, N. Atmospheric nitrogen compounds II: Emissions, transport, transformation, deposition and assessment. *Atmos. Environ.* **2001**, *35*, 1903–1911. [[CrossRef](#)]
5. Zhu, X.; Burger, M.; Doane, T.A.; Horwath, W.R. Ammonia oxidation pathways and nitrifier denitrification are significant sources of N<sub>2</sub>O and NO under low oxygen availability. *Proc. Natl. Acad. Sci. USA* **2013**, *110*, 6328–6333. [[CrossRef](#)]

6. Nielsen, O.K.; Plejdrup, M.S.; Winther, M.; Mikkelsen, M.H.; Nielsen, M.; Gyldenkærne, S.; Fauser, P.; Albrektsen, R.; Hjelgaard, K.H.; Bruun, H.G.; et al. *Annual Danish Informative Inventory Report to UNECE. Emission inventories from the base year of the protocols to year 2015*; Aarhus University DCE — Danish Centre for Environment and Energy: Aarhus, Denmark, 2017. Available online: <http://dce2.au.dk/pub/SR222.pdf> (accessed on 3 December 2020).
7. UNECE. Protocol to Abate Acidification, Eutrophication and Ground-level Ozone. 1999. Available online: [http://www.unece.org/env/lrtap/multi\\_h1.html](http://www.unece.org/env/lrtap/multi_h1.html) (accessed on 25 September 2019).
8. Leith, I.D.; Sheppard, L.J.; Fowler, D.; Cape, J.N.; Jones, M.; Crossley, A.; Hargreaves, K.J.; Tang, Y.S.; Theobald, M.; Sutton, M.R. Quantifying dry NH<sub>3</sub> deposition to an ombrotrophic bog from an automated NH<sub>3</sub> field release system. *Water Air Soil Pollut. Focus* **2005**, *4*, 207–218. [[CrossRef](#)]
9. Wyers, G.P.; Otjes, R.P.; Slanina, J. A continuous-flow denuder for the measurement of ambient concentrations and surface-exchange fluxes of ammonia. *Atmos. Environ.* **1993**, *27*, 2085–2090. [[CrossRef](#)]
10. Sørensen, L.L.; Granby, K.; Nielsen, H.; Asman, W.A.H. Diffusion scrubber technique used for measurements of atmospheric ammonia. *Atmos. Environ.* **1994**, *28*, 3637–3645. [[CrossRef](#)]
11. Hensen, A.; Nemitz, E.; Flynn, M.J.; Blatter, A.; Jones, S.K.; Sørensen, L.L.; Hensen, B.; Pryor, S.C.; Jensen, B.; Otjes, R.P.; et al. Inter-comparison of ammonia fluxes obtained using the Relaxed. *Biogeosciences* **2009**, *6*, 2575–2588. [[CrossRef](#)]
12. Sintermann, J.; Spirig, C.; Jordan, A.; Kuhn, U.; Ammann, C.; Neftel, A. Eddy covariance flux measurements of ammonia by high temperature chemical ionisation mass spectrometry. *Atmos. Meas. Tech.* **2011**, *4*, 599–616. [[CrossRef](#)]
13. Ferrara, R.M.; Carozzi, M.; di Tommasi, P.; Nelson, D.D.; Fratini, G.; Bertolini, T.; Magliulo, V.; Acutis, M.; Rana, G. Dynamics of ammonia volatilisation measured by eddy covariance during slurry spreading in north Italy. *Agric. Ecosyst. Environ.* **2016**, *219*, 1–13. [[CrossRef](#)]
14. Brodeur, J.J.; Warland, J.S.; Staebler, R.M.; Wagner-Riddle, C. Technical note: Laboratory evaluation of a tunable diode laser system for eddy covariance measurements of ammonia flux. *Agric. For. Meteorol.* **2009**, *149*, 385–391. [[CrossRef](#)]
15. Vaittinen, O.; Metsälä, M.; Persijn, S.; Vainio, M.; Halonen, L. Adsorption of ammonia on treated stainless steel and polymer surfaces. *Appl. Phys. B* **2014**, *115*, 185–196. [[CrossRef](#)]
16. Eugster, W.; Senn, W. A cospectral correction model for measurement of turbulent NO<sub>2</sub> flux. *Bound. Layer Meteorol.* **1995**, *74*, 321–340. [[CrossRef](#)]
17. Sintermann, J.; Dietrich, K.; Häni, C.; Bell, M.; Jocher, M.; Neftel, A. A miniDOAS instrument optimised for ammonia field measurements. *Atmos. Meas. Tech.* **2016**, *9*, 2721–2734. [[CrossRef](#)]
18. Flesch, T.K.; Wilson, J.D.; Harper, L.A.; Crenna, B.P.; Sharpe, R.R. Deducing Ground-to-Air Emissions from Observed Trace Gas Concentrations. *J. Appl. Meteorol.* **2004**, *43*, 487–502. [[CrossRef](#)]
19. Häni, C.; Flechard, C.; Neftel, A.; Sintermann, J.; Kupper, T. Accounting for field-scale dry deposition in backward Lagrangian stochastic dispersion modelling of NH<sub>3</sub> emissions. *Atmosphere* **2018**, *9*, 146. [[CrossRef](#)]
20. Kamp, J.N.; Häni, C.; Nyord, T.; Feilberg, A.; Sørensen, L.L. The aerodynamic gradient method: Implications of non-simultaneous measurements at alternating heights. *Atmosphere* **2020**, *11*, 1067. [[CrossRef](#)]
21. Spirig, C.; Flechard, C.R.; Ammann, C.; Neftel, A. The annual ammonia budget of fertilised cut grassland—Part 1: Micrometeorological flux measurements and emissions after slurry application. *Biogeosciences* **2010**, *7*, 521–536. [[CrossRef](#)]
22. Flesch, T.K.; Wilson, J.D.; Harper, L.A. Deducing ground-to-air emissions from observed trace gas concentrations: A field trial with wind disturbance. *J. Appl. Meteorol.* **2005**, *44*, 475–484. [[CrossRef](#)]
23. Loubet, B.; Générmon, S.; Ferrara, R.; Bedos, C.; Decuq, C.; Personne, E.; Fanucci, O.; Durand, B.; Rana, G.; Cellier, P. An inverse model to estimate ammonia emissions from fields. *Eur. J. Soil Sci.* **2010**, *61*, 793–805. [[CrossRef](#)]
24. Sanz, A.; Misselbrook, T.; Sanz, M.J.; Vallejo, A. Use of an inverse dispersion technique for estimating ammonia emission from surface-applied slurry. *Atmos. Environ.* **2010**, *44*, 999–1002. [[CrossRef](#)]
25. Sintermann, J.; Ammann, C.; Kuhn, U.; Spirig, C.; Hirschberger, R.; Gärtner, A.; Neftel, A. Determination of field scale ammonia emissions for common slurry spreading practice with two independent methods. *Atmos. Meas. Tech.* **2011**, *4*, 1821–1840. [[CrossRef](#)]
26. Häni, C.; Sintermann, J.; Kupper, T.; Jocher, M.; Neftel, A. Ammonia emission after slurry application to grassland in Switzerland. *Atmos. Environ.* **2016**, *125*, 92–99. [[CrossRef](#)]
27. Carozzi, M.; Loubet, B.; Acutis, M.; Rana, G.; Ferrara, R.M. Inverse dispersion modelling highlights the efficiency of slurry injection to reduce ammonia losses by agriculture in the Po Valley (Italy). *Agric. For. Meteorol.* **2013**, *171–172*, 306–318. [[CrossRef](#)]
28. Møller, H.B.; Nielsen, K.J. *Biogas Taskforce: Udvikling og Effektivisering af Biogasproduktionen i Danmark DCA Rapport nr. 77*; Aarhus University DCA - Nationalt Center for Fødevarer og Jordbrug, Foulum, Denmark: Tjele, Denmark, 2016. Available online: [https://pure.au.dk/portal/da/persons/henrik-bjarne-moeller\(a2eda86a-cdac-4996-8db0-3cecf51be12\)/publications/biogas-taskforce\(a37f2aac-aa93-4f1b-b644-051ba91b2421\)/export.html](https://pure.au.dk/portal/da/persons/henrik-bjarne-moeller(a2eda86a-cdac-4996-8db0-3cecf51be12)/publications/biogas-taskforce(a37f2aac-aa93-4f1b-b644-051ba91b2421)/export.html) (accessed on 3 December 2020).
29. Kamp, J.N.; Chowdhury, A.; Adamsen, A.P.S.; Feilberg, A. Negligible influence of livestock contaminants and sampling system on ammonia measurements with cavity ring-down spectroscopy. *Atmos. Meas. Tech.* **2019**, *12*, 2837–2850. [[CrossRef](#)]
30. Businger, J.A. Evaluation of the accuracy with which dry deposition can be measured with current micrometeorological techniques. *J. Clim. Appl. Meteorol.* **1986**, *25*, 1100–1124. [[CrossRef](#)]
31. Kljun, N.; Calanca, P.; Rotach, M.W.; Schmid, H.P. A simple two-dimensional parameterisation for Flux Footprint Prediction (FFP). *Geosci. Model Dev.* **2015**, *8*, 3695–3713. [[CrossRef](#)]

32. Edwards, G.C.; Rasmussen, P.E.; Schroeder, W.H.; Wallace, D.M.; Halfpenny-Mitchell, L.; Dias, G.M.; Kemp, R.J.; Ausma, S. Development and evaluation of a sampling system to determine gaseous Mercury fluxes using an aerodynamic micrometeorological gradient method. *J. Geophys. Res. D Atmos.* **2005**, *110*, 1–11. [[CrossRef](#)]
33. Dyer, A.J.; Hicks, B.B. Flux-gradient relationships in the constant flux layer. *Q. J. R. Meteorol. Soc.* **1970**, *96*, 715–721. [[CrossRef](#)]
34. Flesch, T.K. The Footprint for Flux Measurements, from Backward Lagrangian Stochastic Models. *Bound. Layer Meteorol.* **1996**, *78*, 399–404. [[CrossRef](#)]
35. Flesch, T.K.; Wilson, J.D.; Harper, L.A.; Crenna, B.P. Estimating gas emissions from a farm with an inverse-dispersion technique. *Atmos. Environ.* **2005**, *39*, 4863–4874. [[CrossRef](#)]
36. Hafner, S.D.; Pacholski, A.; Bittman, S.; Burchill, W.; Bussink, W.; Chantigny, M.; Carozzi, M.; Générumont, S.; Häni, C.; Hansen, M.N.; et al. The ALFAM2 database on ammonia emission from field-applied manure: Description and illustrative analysis. *Agric. For. Meteorol.* **2018**, *258*, 66–79. [[CrossRef](#)]
37. Kljun, N.; Kormann, R.; Rotach, M.W.; Meixner, F.X. Comparison of the Lagrangian footprint model LPDM-B with an analytical footprint model. *Bound. Layer Meteorol.* **2003**, *106*, 349–355. [[CrossRef](#)]
38. Bell, M.; Flechard, C.; Fauvel, Y.; Häni, C.; Sintermann, J.; Jocher, M.; Menzi, H.; Hensen, A.; Neftel, A. Ammonia emissions from a grazed field estimated by miniDOAS measurements and inverse dispersion modelling. *Atmos. Meas. Tech.* **2017**, *10*, 1875–1892. [[CrossRef](#)]
39. Sutton, M.A.; Milford, C.; Nemitz, E.; Theobald, M.R.; Hill, P.W.; Fowler, D.; Schjoerring, J.K.; Mattsson, M.E.; Nielsen, K.H.; Husted, S.; et al. Biosphere-atmosphere interactions of ammonia with grasslands: Experimental strategy and results from a new European initiative. *Plant Soil* **2001**, *228*, 131–145. [[CrossRef](#)]
40. Laubach, J.; Kelliher, F.M. Measuring methane emission rates of a dairy cow herd by two micrometeorological techniques. *Agric. For. Meteorol.* **2004**, *125*, 279–303. [[CrossRef](#)]
41. Beauchamp, E.G.; Kidd, G.E.; Thurtell, G. Ammonia volatilization from liquid dairy cattle manure in the field. *Can. J. Soil Sci.* **1982**, *62*, 11–19. [[CrossRef](#)]
42. Sommer, S.G.; Générumont, S.; Cellier, P.; Hutchings, N.J.; Olesen, J.E.; Morvan, T. Processes controlling ammonia emission from livestock slurry in the field. *Eur. J. Agron.* **2003**, *19*, 465–486. [[CrossRef](#)]
43. Hansen, M.N.; Sommer, S.G.; Hutchings, N.J.; Sørensen, P. Emission factors for calculation of ammonia volatilization by storage and application of animal manure. *J. Agric. Sci.* **2018**, *156*, 1070–1078. [[CrossRef](#)]
44. Nelson, A.J.; Lichiheb, N.; Koloutsou-Vakakis, S.; Rood, M.J.; Heuer, M.; Myles, L.T.; Joo, E.; Miller, J.; Bernacchi, C. Ammonia flux measurements above a corn canopy using relaxed eddy accumulation and a flux gradient system. *Agric. For. Meteorol.* **2019**, *264*, 104–113. [[CrossRef](#)]
45. Vesala, T.; Kljun, N.; Rannik, Ü.; Rinne, J.; Sogachev, A.; Markkanen, T.; Sabelfeld, K.; Foken, T.; Leclerc, M.Y. Flux and concentration footprint modelling: State of the art. *Environ. Pollut.* **2008**, *152*, 653–666. [[CrossRef](#)] [[PubMed](#)]